Journal of Magnetic Resonance 198 (2009) 160–166

Contents lists available at ScienceDirect

Journal of Magnetic Resonance

journal homepage: www.elsevier.com/locate/jmr

Measurement of glutathione in human brain at 3T using an improved double quantum filter *in vivo*

Changho Choi [a,*], Chenguang Zhao [a], Ivan Dimitrov [a,b], Deborah Douglas [a], Nicholas J. Coupland [c], Sanjay Kalra [d], Halima Hawesa [a], Jeannie Davis [a]

[a] *Advanced Imaging Research Center, University of Texas Southwestern Medical Center, 5323 Harry Hines Blvd., Dallas, TX 75390, USA*
[b] *Philips Medical Systems, Cleveland, OH, USA*
[c] *Psychiatry, University of Alberta, Edmonton, AB, Canada*
[d] *Neurology, University of Alberta, Edmonton, AB, Canada*

ARTICLE INFO

Article history:
Received 4 August 2008
Revised 5 February 2009
Available online 13 February 2009

Keywords:
Double quantum filtering
Dual DQC encoding
Glutathione
Human brain

ABSTRACT

A single voxel proton NMR double quantum filter (DQF) for measurement of glutathione (GSH) in human brain at 3T is reported. Yield enhancement for the CH_2 resonances of the cysteine moiety at 2.95 ppm has been achieved by means of dual encoding. After the preparation of double quantum and zero quantum coherences (DQC and ZQC) at equal magnitude, the first DQC encoding was followed by interchange of DQC and ZQC, and another DQC encoding. The multi-quantum coherences were fully utilized to generate a GSH target signal at ~2.95 ppm. The optimal echo time and the editing efficiency were obtained with numerical analysis of the filtering performance and phantom measurements. The dual-DQC encoding method provided GSH yield greater by a factor of 2.1 than single-DQC encoding for identical slice-selective RF pulses in phantom tests. Using the phantom relaxation times and the ratio of edited GSH to *N*-acetylaspartate (NAA) 2.0-ppm peak areas, the concentration of GSH in the medial parietal cortex of the healthy human brain in vivo was estimated to be 1.0 ± 0.3 mM (mean ± SD, n = 7), with reference to NAA at 10 mM.

1. Introduction

Glutathione (GSH), a primary antioxidant, plays an important role in protecting reactive molecules in living cells against oxidative damage [1]. Altered GSH concentrations in the human brain have been reported in several pathological diseases such as schizophrenia [2] and cancer [3], as measured by proton nuclear magnetic resonance spectroscopy (MRS). Accurate evaluation of the GSH level in vivo is therefore of great clinical significance. GSH is a tripeptide, consisting of glycine, cysteine and glutamate. Although its concentration in the human brain is not extremely low (1–3 mM), precise measurement of GSH by conventional MRS is quite difficult due to the severe spectral overlap with much more intense signals of creatine (Cr), glutamate (Glu) and the aspartyl moiety of *N*-acetylaspartate (NAA) [4]. The majority of the GSH and other interfering metabolite resonances are strongly coupled, complicating the spectral analysis. Short-TE approaches benefit from reduced T_2 signal loss [5] but add the penalty of spectral overlap with Cr and macromolecule (MM) signals [6]. Long echo times with appropriate TE optimization can improve the selectivity of the target multiplet and reduce the MM signal, yet allow measurement of the target multiplet within a clinically acceptable time frame [7–9]. In both approaches, exceptionally good shimming and a high signal-to-noise ratio are required to reliably differentiate the small GSH signal from the abundant interfering resonances.

Alternatively, spectral editing can be employed to reveal low-abundance metabolite signals by eliminating overlapping signals [10,11]. Due to the close proximity of the GSH Glu moiety resonances to the neighboring resonances and their strong coupling features [4], the cysteine (Cys) moiety of GSH has been commonly targeted in prior editing studies. These include scalar difference editing [12,13] and double quantum filtering (DQF) [14–16]. Both methods filter out a GSH Cys signal at ~2.95 ppm via selective excitation of the weak-coupling partner at 4.56 ppm, while eliminating the Cr 3.03 ppm singlet which is the major overlapping resonance. Following the application of a standard DQF strategy to GSH measurements [14,15], Zhao et al. proposed a DQF design [16], whereby a GSH signal was generated via two spectrally selective 90° pulses split by a slice-selective 180° pulse without the need of phase optimization of the DQC generating 90° RF pulse. In these prior methods, following the preparation of double quantum and zero quantum coherences (DQC and ZQC) at equal magnitude, only DQC was selected for editing, leading to a GSH signal smaller than that achievable by the difference editing.

* Corresponding author. Fax: +1 214 645 2885.
E-mail address: changho.choi@utsouthwestern.edu (C. Choi).

1090-7807/$ - see front matter © 2009 Elsevier Inc. All rights reserved.
doi:10.1016/j.jmr.2009.02.002

Here, we report a modified DQF sequence that enables enhancement of the GSH by means of dual DQC encoding [17,18], whereby DQC and ZQC are both utilized for detection of GSH at 2.95 ppm. After a DQC encoding, a spectrally selective 180° pulse is employed to interchange the DQC and ZQC, followed by an additional DQC encoding. The performance of the strategy for GSH measurement is demonstrated with density-matrix simulations and phantom data. Finally, the method was applied in seven healthy volunteers to obtain a measure of GSH in the human parietal cortex.

2. Materials and methods

2.1. RF sequence

The cysteine moiety of GSH can be modeled as an ABX spin system, with resonances at 2.93, 2.97 and 4.56 ppm, respectively, and coupling strengths of $(J_{AB}, J_{AX}, J_{BX}) = (-14.1, 7.1, 4.7)$ Hz [4]. The strongly coupled AB spins can be edited using a volume-selective double quantum filtering (DQF) sequence, as illustrated in Fig. 1. Following a slice-selective 90° excitation pulse, the in-phase coherences of the three spins evolved to antiphase coherences during the first echo period TE_1, including $A_{\pm}X_0$, $B_{\pm}X_0$, $A_{\pm}B_0X_0$ and $A_0B_{\pm}X_0$, which were edited to give rise to a target signal at ~2.95 ppm. A single-band 90° RF pulse (S90), tuned to the X spin at 4.56 ppm, was applied at the end of TE_1, converting the antiphase coherences to DQC and ZQC at equal magnitude. Following DQC encoding by a gradient pulse G_1, a dual-band 180° pulse (D180) was applied for selective 180° rotation of the 4.56 ppm resonance without affecting the *A* and *B* spins. Consequently, the DQC and ZQC coherences were interchanged, which was immediately followed by another DQC encoding gradient G_2. The encoded coherences are then converted to A- and B-spin antiphase coherences with the second S90 pulse. The J evolution during TE_2 and a decoding gradient G_3 applied after the slice-selective 180° pulse brought about a GSH signal at 2.95 ppm. The gradient areas were set as $G_3 = 2G_1 = 2G_2$.

Cr, GABA and MM have resonances that overlap with the GSH AB spin resonances at 2.95 ppm, but do not have coupling partners in the proximity of the GSH X spin resonance (4.56 ppm) and consequently their coediting is entirely prevented. However, the aspartate (Asp) moieties of NAA and NAAG and the Asp molecules have resonances in the vicinity of 2.95 and 4.56 ppm, so these compounds may interfere with the GSH editing. Suppression of these compounds was achieved by means of the D180 pulse, whose inversion profile is shown in Fig. 2. The bandwidth of this 20-ms Gaussian D180 was 51 Hz at half amplitude, causing partial excitation at the CH resonances of NAA (42% at 4.38 ppm) and NAAG (94% at 4.61 ppm). The D180 pulse was designed to excite their coupling partners at 2.5–2.7 ppm (CH_2 resonances) without affecting the GSH AB spin resonances. Hence, the DQC and ZQC of GSH at the beginning of the TM period underwent interchange as described above, but those of NAA and NAAG were largely preserved following the D180, with opposite quantum numbers for both CH and CH_2 protons, i.e., $A_+X_+ \rightarrow A\_X\_$. Thus, the effects of G_1 and G_2 on the DQC are canceled and the coherences are eventually dephased by gradient G_3 in TE_2. For Asp, the CH resonance at 3.89 ppm was not affected by the D180 so there is no contribution to the CH_2 resonance at ~2.8 ppm.

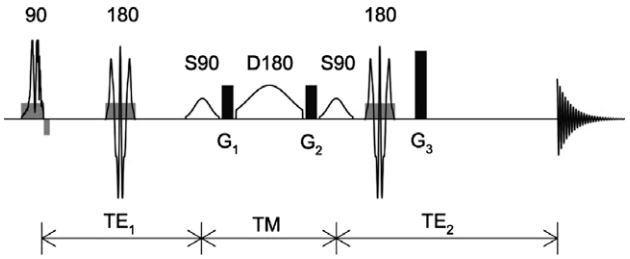

Fig. 1. Schematic diagram of the GSH DQF sequence. Three spectrally selective RF pulses (S90, D180 and S90) were applied between the two slice-selective 180° pulses of a PRESS sequence. Single-band 90 pulses (S90) were tuned to the GSH 4.56-ppm resonance. A dual-band 180° pulse (D180), applied between the S90 pulses, was tuned to 4.56 and 2.43 ppm, having no effect on the GSH 2.95-ppm resonance. The first encoding gradient (G_1) encoded the DQC following the first S90, and the gradient G_2 encoded the DQC converted from the ZQC by D180. The second S90, tuned to 4.56 ppm, converted the encoded DQCs into antiphase coherences, which were decoded with G_3 (=$2G_1 = 2G_2$) during TE_2. The sequence times TE_1, TM and TE_2 were 51, 36, and 62 ms, respectively. The second slice-selective 180° pulse was applied at $(TE_2 - TM)/2$ from the center of the second S90 pulse, to refocus the B_0 inhomogeneity effect from TM in the TE_2 period. Spoiling gradients were applied symmetrically about the slice-selective 180° pulses (not drawn for simplicity).

2.2. RF phases of S90 and D180

Since the first S90 pulse influences the X spin only, the antiphase to multi-quantum coherence conversion is fully accomplished regardless of the RF phase of the S90 pulse. This implies that the maximum GSH edited signal can be obtained irrespective of the RF phase of the coherence conversion pulse, as opposed to the prior DQF sequence [14,15]. However, this is the case only when the second S90 pulse which induces the multi-quantum to antiphase coherence conversion retains certain phase coherences with respect to that of the first S90 pulse. For the GSH DQF sequence of the present study

$$90_{\varphi 1} - 180_{\varphi 2} - S90_{\varphi 3} - D180_{\varphi 4} - S90_{\varphi 5} - 180_{\varphi 6},$$

the RF phase factors of the observable coherence terms having a quantum number of −1 at the acquisition [19] may be given by

$$\exp[i(\varphi_1 - 2\varphi_2 - \varphi_3 + 2\varphi_4 - \varphi_5 + 2\varphi_6)] \quad (1a)$$

$$\exp[i(\varphi_1 - 2\varphi_2 + \varphi_3 - 2\varphi_4 + \varphi_5 + 2\varphi_6)]. \quad (1b)$$

The present GSH editing requires S90 RF phases that add the terms (1a) and (1b) constructively. The two terms exhibit only a phase difference arising from the S90 and D180 pulses, i.e.,

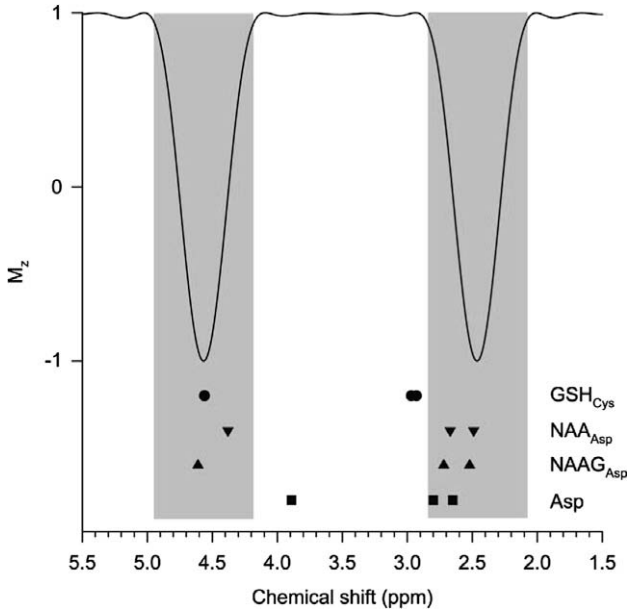

Fig. 2. The inversion profile of the dual-band 180° pulse (D180). The positions of the GSH cysteine moiety resonances and of the interfering signals (NAA, NAAG and Asp) are depicted, showing the extent to which the different resonances are affected by the D180 pulse.

$\exp(-i\theta)$ and $\exp(i\theta)$ with $\theta = \varphi_3 - 2\varphi_4 + \varphi_5$. These two phase factors are equal when $\theta = n\pi$, with $n = 0, \pm1, \pm2$, etc. Adopting orthogonal phases for RF pulses (i.e., 0, $\pi/2$, π or $3\pi/2$), the phases of the two S90 pulses should be such that $\varphi_3 + \varphi_5 = n\pi$. This indicates that $(\varphi_3, \varphi_5) = (\pi/2, \pi/2)$ and $(\pi/2, -\pi/2)$, for an example, are both acceptable. In practice, the former is preferred because it gives rise to a GSH signal with polarity opposite to that from $(\varphi_3, \varphi_5) = (0, 0)$, and can be utilized to eliminate the overlapping Cr 3.03 ppm resonance. The Cr resonance is not influenced by the S90 pulse, and consequently the signal remains the same. Hence, a receiver phase shift by 180° will cancel the Cr resonance while adding the GSH signals constructively. In addition, constructive addition of the GSH signal can also be accomplished with the D180 phase cycling at 0 and $\pi/2$ and the receiver phase at 0 and π, respectively. For in vivo use, a 512-step phase cycling scheme was constructed which incorporates four steps of φ_1, φ_2, φ_3 and φ_4, and two steps (0 and $\pi/2$) of φ_6. The phase φ_5 was set equal to φ_3.

2.3. Numerical optimization of sequence times

A density-matrix simulation [10] was carried out to optimize and evaluate the performance of the DQF sequence. The published chemical shift and coupling constants [4] were used. The calculation incorporated the full Hamiltonian that included the Zeeman, chemical shift and scalar coupling terms, and the shaped RF and gradient pulses. The density operator evolution during the slice-selective and spectrally selective RF pulses was all calculated with transformation matrices [9,10,20]. The spatial resolution of 3D volume localization was set at 1%. The second echo time TE_2 was set such that the coherence evolution due to the B_0 inhomogeneity effect during the mixing time TM can be refocused at the end of TE_2 [21]. The 180° pulse was applied at $(TE_2 - TM)/2$ from the beginning of TE_2. The GSH editing was simulated for sequence times TE_1 = 20–100 ms, TM = 36–100 ms, and TE_2 = 62–100 ms, with increments of 1 ms. Here, the smallest values (TE_1, TM, TE_2) = (20, 36, 62) ms were the shortest possible timings for the given durations of RF and gradient pulses. The amplitude of the GSH edited multiplet was maximal at (TE_1, TM, TE_2) = (51, 36, 62) ms. The yield of the volume-selective DQF sequence was calculated with respect to the signal intensity of a volume-selective 90° -acquisition. A volume-selective 90° -acquired spectrum of GSH for the same localized volume as in the simulation of the DQF sequence was obtained by multiplying the 90° -acquired spectrum of the entire sample volume by a voxel to entire volume ratio, which was obtained from a signal ratio of an uncoupled spin system between volume-selective and non-selective sequences. From the area of the GSH AB-spin multiplet, the yield of the DQF sequence was estimated as 0.49. The amplitude of the DQF multiplet was 0.53 relative to that of the volume-selected 90° -acquired multiplet for a linewidth of 5 Hz, a typical in vivo linewidth at 3T. Effects due to NMR relaxation and molecular diffusion were not included in the calculation. The density-matrix simulation was programmed with Matlab (The MathWorks Inc.).

2.4. Experimental

Experiments were carried out on a 3.0 T whole-body Philips scanner with dual QUASAR high performance gradient coils (maximum gradient strength 80 mT/m; slew rate 200 mT/m/ms) (Philips Medical Systems, Cleveland, Best, The Netherlands). A standard quadrature birdcage coil was used for both RF transmission and reception. The maximum available RF field intensity (B_1) was 20 μT. The spatial localization part of the DQF sequence consisted of a 90° RF pulse (amplitude- and frequency-modulated; 6.6 ms; BW = 6.3 kHz) and two 180° RF pulse (amplitude modulated; 8.9 ms; BW = 1.9 kHz). The spectrally selective single-band 90° RF pulse (S90) had a 10 ms Gaussian envelope (truncated at 10%). A dual-band 180° pulse (D180), applied between the S90 pulses, was a 20 ms Gaussian waveform (truncated at 26%) that incorporated successive RF phase variation [22] designed for refocusing at 4.56 and 2.43 ppm. The excitation bandwidth was 200 and 51 Hz for S90 and D180 pulses, respectively. The gradient pulse duration was 3 ms in all cases.

The filtering sequence was tested on a spherical phantom (i.d. = 6 cm), containing GSH (99 mM), NAA (50 mM), and glycine (Gly) (31 mM) in water. Proton spectra following the DQF sequence were acquired from a single voxel ($25 \times 30 \times 30\ mm^3$) with TR = 15 s (>$6T_1$ for the phantom solution). In order to estimate the DQF yield of the proposed sequence experimentally, relaxation times (T_1 and T_2) of GSH and NAA were measured on this phantom. T_2's of the GSH 2.95 and NAA 2.0 ppm resonances were measured using a volume-localized spectrally selective triple refocusing sequence (i.e., 90°–180°–180°–180°), where the second 180° pulse (55 ms; BW = 296 Hz; tuned to 2.8 ppm) refocused the GSH and NAA resonances but dephased the GSH 4.56 ppm resonance. Spectra were obtained at three TE values (TE = 124, 204 and 264 ms). The NAA data were fitted with a mono-exponential function for T_2 estimation. For GSH, the data were fitted with density matrix calculated peak area values multiplied by a mono-exponential function. T_1 was measured with an inversion recovery method. In addition, comparison of the present dual-DQC encoding sequence and the recently reported single-DQC encoding method [16] was carried out on a phantom with GSH (10 mM), NAA (51 mM), and Gly (10 mM). Two sequences were designed for the single-DQC encoding method; one with the same slice-selective 180° pulse as in the proposed sequence and another with a 4-ms optimized slice-selective 180° pulse (BW = 1.1 kHz; 5 lobes) generated from MATPULSE [23]. The sequence times were (TE_1, TM, TE_2) = (15, 21.5, 70) and (10, 16.5, 70) ms, respectively, for the sequence in Fig. 1 of Ref. [16].

In vivo tests of the DQF filter were conducted on seven healthy volunteers, aged 20–40 years. Written informed consent was obtained prior to the scans. A $25 \times 33 \times 33\ mm^3$ voxel was positioned in the parietal cortex. Second-order shimming for the selected volume was carried out using FASTMAP [24]. DQF spectra were acquired using TR = 2 s, TE = 149 ms, sweep width = 2.5 kHz, number of sampling points = 2048, and number of averages = 512. A variable-flip-angle water suppression subsequence [25], with four 28 ms long Gaussian RF pulses separated by spoilers, was applied prior to the filtering sequence. The carrier of the volume-selective RF pulses was set to 3.0 ppm. The acquisition was comprised of 128 subscans, each with four averages without change in S90 and D180 phases. The residual eddy current effect on the acquisition was removed by correcting the phase of the individual data points of each FID, using the phase factor of the water FID acquired with an identical gradient scheme.

The frequency drift during the measurement was minimized first by acquiring the STEAM water signal from the localized volume using a small flip angle (<5°) and then re-setting the synthesizer frequency prior to each single scan. This was completed within 12 ms. Using this method, the residual frequency drift during the 17 min GSH measurement was within ±2 Hz. The mean standard deviation (SD) of the residual frequency drift was 0.3 Hz, with a maximum SD < 0.4 Hz. Each FID was then apodized with a 3 Hz exponential function before Fourier transformation. The spectra in each of 128 subscans were corrected for frequency drift and phase individually in the frequency domain, using the NAA and Cr signals as a reference. The NAA singlet of the DQF subspectra, which were obtained without the phase cycling of S90 and D180, was used as a reference for in vivo GSH estimation, incorporating the T_1 and T_2 of GSH and NAA in an aqueous solution.

3. Results

Fig. 3 presents numerically calculated 3D-localized spectra of GSH, NAA, NAAG and Asp for 90° -acquisition and DQF with (TE_1, TM, TE_2) = (51, 36, 62) ms. Compared to the 90° -acquired signal, the yield of the dual-encoding DQF is 53% and 49% in terms of peak amplitude and area. For an identical concentration, the 90° -acquired signals of NAA, NAAG and Asp are comparable to that of GSH, but these interfering resonances are suppressed drastically following the filtering sequence, their peak amplitude being 7%, 15% and 4% with respect to the GSH edited peak intensity. This excellent suppression of these interfering metabolites is due to the D180 pulse which excites both CH and CH_2 resonances of the interfering aspartyl groups during the TM period. Spectra scaled for a typical brain concentration ratio of [GSH]:[NAA]:[NAAG]:[Asp] = 1:9:2:1 are also shown in Fig. 3. For a spectral region indicated by vertical lines (0.2 ppm width), the sum of the residual peak areas of the interferences is ~1% with respect to the GSH peak area, so the GSH signal intensity can be obtained directly from the peak area calculation with negligible contamination, removing the need for spectral fitting. For comparison, when the D180 is replaced with a single-band 180° pulse with an identical excitation bandwidth, the coedited signal amplitude of NAA and NAAG both increases by a factor of ~3 and as a result, the interferences-to-GSH peak area ratio becomes ~60%. The Cr signal is canceled following the phase cycling of the S90 and D180 pulses, as described earlier.

Fig. 4 illustrates phantom T_2 measurements for the NAA 2.0 and GSH 2.95 ppm resonances. From a mono-exponential fitting, the NAA T_2 was measured as 980 ms. For GSH, a density-matrix simulation indicated that, despite the selective J rewinding by the second 180° pulse of the triple refocusing sequence, the signal from the strongly coupled spins decreases with TE [26]. Fitting the phantom data with the calculated TE dependence combined with $\exp(-TE/T_2)$ gave a GSH T_2 as 510 ms. The T_1's of GSH and NAA in the phantom solution were measured as 0.45 and 1.5 s, respectively, in good agreement with literature values for human brain [27,28].

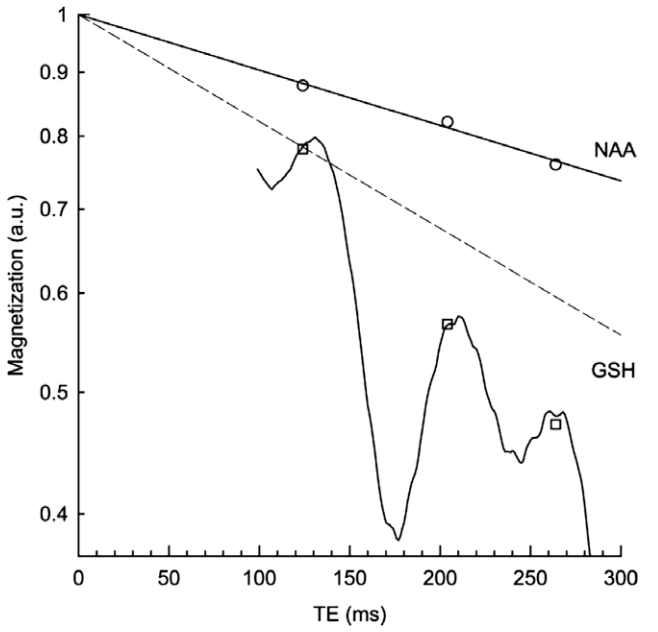

Fig. 4. Phantom T_2 measurements of GSH (2.95 ppm) and NAA (2.0 ppm), using a 90°–180°–180°–180° sequence, where the second 180° pulse was spectrally selective, refocusing the GSH 2.95-ppm and NAA singlet resonances and dephasing the GSH 4.56-ppm resonance. A mono-exponential fitting of the NAA data (circle) gave an NAA T_2 of 980 ± 120 ms. For GSH, the numerically calculated TE dependence pattern of the 2.95 ppm resonances combined with $\exp(-TE/T_2)$ was fitted to the data (square), leading to a GSH T_2 of 510 ± 40 ms (solid line). The mono-exponential function with this T_2 is drawn (dashed line) for comparison with the NAA TE dependence. The repetition time (TR) was 15 s.

Fig. 5 shows phantom and calculated spectra of GSH, NAA and Gly, for the single-voxel localized DQF sequence. The spectral pattern and signal intensities are in good agreement between experiment and simulation. The phantom spectra indicate that the area of the GSH filtered multiplet is 0.239 with respect to the NAA peak area for a GSH-to-NAA concentration ratio of 1:1. This is smaller

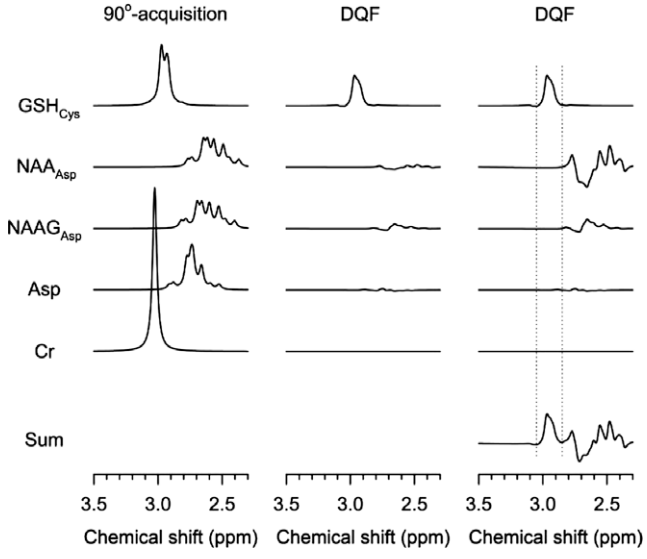

Fig. 3. Calculated spectra of GSH, NAA, NAAG, Asp and Cr at equal concentrations, following a 90° -acquisition (left) and DQF sequences (middle). The DQF spectra for a physiologically relevant concentration ratio [GSH]:[NAA]:[NAAG]:[Asp]:[Cr] = 1:9:2:1:8 are also shown (right), together with their sum. The spectra were broadened with a 5-Hz exponential function. Vertical lines represent the width for peak area calculation in vivo.

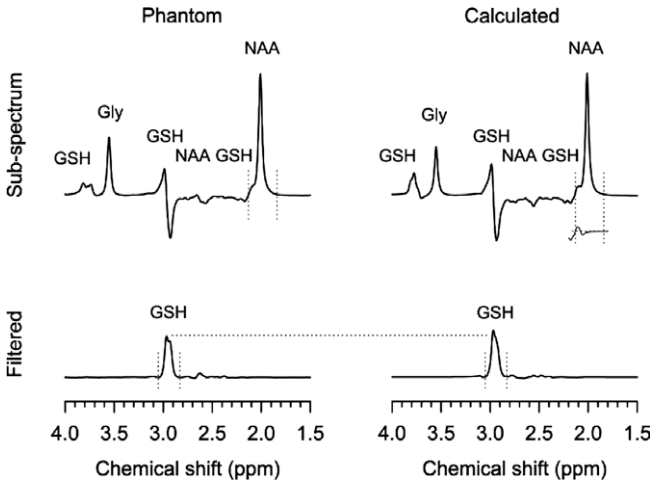

Fig. 5. Phantom and calculated spectra of GSH, NAA and Gly at concentrations of 99, 50 and 31 mM, respectively, obtained with the single-voxel localized DQF sequence. Subspectra were obtained without phase cycling of S90 and D180 pulses. Vertical lines indicate the spectral region for peak area calculation for GSH and NAA. The NAA signal overlaps with the GSH glutamate multiplet at ~2.0 ppm, but the GSH multiplet itself has a null area within the vertical lines and consequently its contribution to the NAA peak area is negligible, as indicated by a separate display of the calculated GSH glutamate signal. Spectra are broadened to 5 Hz. TR was 15 s in the phantom test.

than the calculated (without the T_2 effect) (0.279), as indicated by the horizontal dashed line. Extrapolation of the experimental signal ratio to zero TE using the phantom T_2's of GSH and NAA reproduces the calculated signal ratio when the GSH T_2 for the TM period is set at 420 ms, i.e.,

$$0.239 = 0.279\frac{\exp\left[-(\mathrm{TE}_1+\mathrm{TE}_2)/T_{2,\mathrm{GSH}}\right]\exp\left[-\mathrm{TM}/T_{2,\mathrm{GSH,TM}}\right]}{\exp\left[-(\mathrm{TE}_1+\mathrm{TM}+\mathrm{TE}_2)/T_{2,\mathrm{NAA}}\right]}, \quad (2)$$

where $T_{2,\mathrm{GSH,TM}}$ = 420 ms and (TE_1, TM, TE_2) = (51, 36, 62) ms. This estimated TM T_2 of GSH is about 20% shorter than the measured GSH single-quantum T_2.

Fig. 6 displays in vivo brain dual-encoding DQF spectra, obtained from the parietal cortex of seven healthy volunteers. The filtered spectra are shown together with subspectra for each subject. A small GSH edited peak is detected at 2.95 ppm consistently in all filtered spectra. The extent of elimination of potential Cr contamination can be judged by the complete suppression of the NAA 2.0-ppm singlet which undergoes similar cancellation. The GSH concentration was calculated from the peak areas of the GSH filtered and the subspectral NAA 2.0-ppm signals. The GSH-to-NAA peak area ratio ξ was measured as 0.02 ± 0.005 (mean ± SD, n = 7) in a steady-state mode (TR = 2 s). A density-matrix simulation gave a GSH-to-NAA peak area ratio (ξ') of 0.279 for equal concentrations without relaxation effects. Incorporating the phantom T_1's of GSH and NAA to correct the T_1 effect (as noted earlier, the T_1's in the phantom were similar to in vivo values) and assuming that the GSH-to-NAA T_2 ratio of the phantom is representative of this ratio in the brain, the GSH concentration for brain was estimated, using an equation

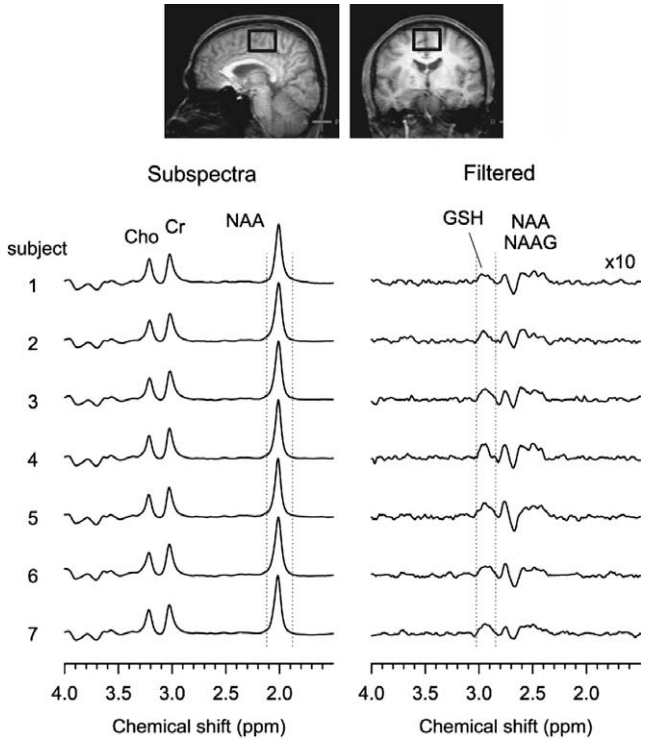

Fig. 6. A stack of in vivo spectra, obtained from six healthy subjects, is presented, together with the voxel positioning. The DQF spectra from each subject are scaled with respect to the NAA 2.0 ppm singlet of the DQF subspectra. The GSH spectra are magnified 10 times. The spectra were all apodized with a 3-Hz exponential function, leading to a mean signal-to-background noise ratio of 9 for GSH. The experimental parameters were TR = 2 s, TE = 113 ms, TM = 36 ms and NEX = 256 (subspectra), 512 (GSH). The peak area was calculated between the vertical lines.

$$[\mathrm{GSH}] = [\mathrm{NAA}]\frac{\xi}{\xi'}\frac{1-\exp(-\mathrm{TR}/T_{1,\mathrm{NAA}})}{1-\exp(-\mathrm{TR}/T_{1,\mathrm{GSH}})} \times \frac{\exp[-(\mathrm{TE}_1+\mathrm{TM}+\mathrm{TE}_2)/T_{2,\mathrm{NAA}}]}{\exp[-(\mathrm{TE}_1+\mathrm{TE}_2)/T_{2,\mathrm{GSH}}]\exp(-\mathrm{TM}/T_{2,\mathrm{GSH,TM}})}, \quad (3)$$

to be 1.0 ± 0.3 mM, for [NAA] = 10 mM. Here, $T_{1,\mathrm{NAA}}$ = 1.5 s, $T_{1,\mathrm{GSH}}$ = 0.45 s, $T_{2,\mathrm{NAA}}$ = 250 ms [28], $T_{2,\mathrm{GSH}}$ = 250 × (510/980), and $T_{2,\mathrm{GSH,TM}} = T_{2,\mathrm{GSH}} \times$ (420/510). The GSH concentration is in good agreement with prior studies [12,16].

4. Discussion

Despite the signal enhancement by dual-DQC encoding, the yield of the reported filtering sequence is ~50% with respect to 90° -acquisition. Two major sources of signal loss are present. First, substantial signal loss occurs due to voxel displacement effects [29]. The excitation bandwidth (6.3 kHz) of the slice-selective 90° RF pulse is large compared to the spectral distance (206 Hz) between the AB- and X-spin resonances of the GSH cysteine moiety, so the voxel shift during the 90° pulse is negligible. However, the signal loss due to the limited bandwidth (1.9 kHz) of the two slice-selective 180° pulses is quite considerable. The slice displacement of the GSH resonances is approximately 11% (=206/1900). This appears to be responsible for ~25% signal reduction from the 90° -acquired signal intensity, as concluded from a numerical simulation. Another source of signal loss is due to the destructive coherence evolution during the TM period. A computer simulation indicates that the GSH edited signal intensity decreases with increasing TM. Thus, a further signal enhancement can be achieved using short selective pulses in TM. For example, S90 and D180 pulses can be designed at 5 ms for GSH editing, giving signal enhancement by ~20% compared to the reported sequence. This signal increase is due to the reduced deleterious coherence evolution during the RF pulses as well as the reduced TM. However, these pulses have greater excitation bandwidth and consequently will cause a penalty of substantially increased background signals in vivo. For comparison, without the D180 and the second encoding gradient, TM can be reduced to 13 ms, but the maximum achievable peak amplitude from this single-DQC encoding is only 24% at (TE_1, TM, TE_2) = (74, 13, 37) ms, relative to 90° -acquisition. It is noteworthy that the optimal TE_1 and TE_2 depend on TM and also on the type of spectrally selective RF pulses. Optimization of the echo times is critical to minimize the deleterious effect of the finite TM period.

The GSH editing yield depends on the waveform and the duration of the slice-selective RF pulses. Their minimum duration is desirable because it reduces both the destructive coherence proliferation and the voxel displacement due to the increased BW. The slice-selective 180° pulse (amplitude modulated) of the present study has bandwidth of 1.9 kHz at the maximum available RF intensity B_1 = 20 μT. An amplitude/frequency-modulated (non-adiabatic) RF pulse is available [30], which gives much greater refocusing BW (3.2 kHz) at the same B_1 and a duration of 11.4 ms. A computer simulation shows that, despite its bandwidth larger by 70%, the maximum achievable GSH peak from this pulse is only 3% greater at (TE_1, TM, TE_2) = (54, 36, 64.5) ms than in the present study. Here, TE_2 is longer because of the increased duration of the 180° pulse. The reduced signal gain from this greater-bandwidth RF pulse is due largely to the presence of the substantial dispersion component in the refocusing profile (data not shown) and partially to the longer TE_2. This small signal enhancement with the increased echo time (by 5.5 ms) will not be beneficial in vivo because of the T_2 effect.

A phantom comparison between the present dual-DQC encoding and the published single-DQC encoding [16] is illustrated in Fig. 7. As shown, the dual encoding sequence gives a GSH signal

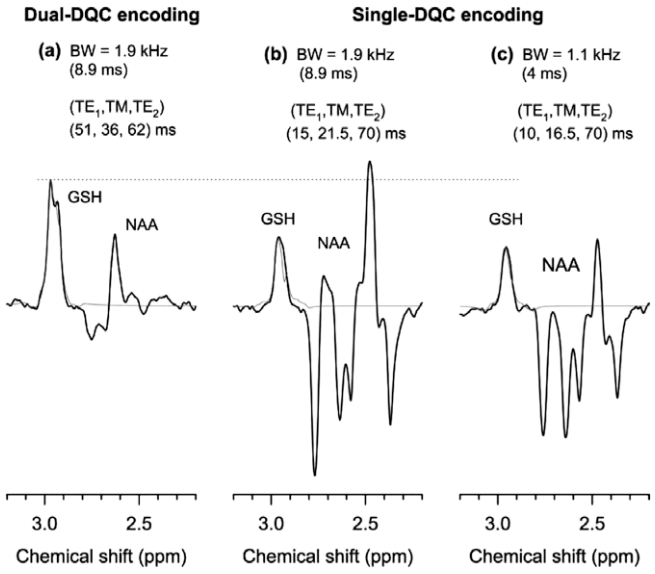

Fig. 7. Phantom (thick line) and simulation (thin line) comparison of the dual-DQC encoding sequence (a) and the published single-DQC encoding method [16] for two types of slice-selective 180° pulses (b and c). The 180° pulse in (b) was the same as in (a). The 180° pulse in (c) was a 4-ms 5-lobe optimized pulse [23], with a smaller bandwidth (1.1 kHz). TR was 15 s (>5T_1) in the phantom test. Spectra were broadened to 5 Hz and normalized with respect to the NAA singlet obtained with PRESS (TE = 149 ms) for individual slice-selective 180° pulses. The concentrations of GSH and NAA were 10 and 50 mM, respectively.

2.1 and 2.7 times greater than the single encoding method in terms of peak amplitude and area, respectively, see Fig. 7a and c. Signal loss due to the voxel displacement effect in Fig. 7c is substantial and consequently, despite the shorter sequence time, the signal is more than twice smaller than that of Fig. 7a. When an 8.9-ms slice-selective 180° pulse that has bandwidth greater by 70% is implemented in the single encoding scheme [16] to make the voxel shift artifact identical, the benefit from the increased bandwidth is balanced out by the deleterious effect of the increased TM, thereby leading to a marginal increase in yield. The ratios of peak amplitude and area between Fig. 7a and b are 1.8 and 2.1, respectively. This ~2-fold signal enhancement for an identical slice-selective 180° RF pulse indicates that the DQC-ZQC interchange occurs during the TM 180° pulse completely. However, signal gain of the dual-DQC encoding may be reduced in vivo due to the large relaxation effects during the long TM.

A potential problem with the in vivo application of an editing sequence having a narrow-band RF pulse is that the signal is sensitive to frequency drifts due primarily to subject motions. This effect depends on the degree of the frequency drift and the bandwidth of the editing pulses. Re-setting the synthesizer frequency prior to each scan turned out to be very efficient, leading to residual drift of no more than ±2 Hz during the 17 min scan. This small drift does not influence the GSH edited signal substantially. The D180 pulse whose bandwidth is smaller (51 Hz) gives 180° rotation of >99.9% at ±2 Hz. A numerical simulation indicates that, for frequency changes of ±1 and ±2 Hz, the GSH signal reduces by 0.15% and 0.4%, respectively. The reported method utilizes three spectrally selective RF pulses to generate a GSH target signal and cancel the overlapping resonances. The performance of the RF pulses may be degraded when B_1 is inhomogeneous as encountered in a surface coil or chemical shift imaging application [27].

The proposed sequence generates a GSH target signal at 2.95 ppm in a single shot by means of double quantum filtering. The overlapping resonances (e.g., Cr 3.03 ppm) are eliminated via subtraction between subspectra, while the GSH signal accumulates constructively. The majority (~99%) of the Cr 3.03 ppm signal is removed with this subtraction, and additional mechanisms are involved in further suppression of unwanted resonances. Excitation of the Cr spins by S90 and D180 is not completely null (⩽1%). Thus, a small fraction of the Cr transverse magnetization at the end of TE_1 is affected by S90 and becomes longitudinal at the beginning of the TM period. This magnetization is destroyed, whether influenced by D180 or not, due to the effects of the encoding and decoding gradients. For the transverse magnetization of Cr at the beginning of TM, the majority is transparent to the D180 (see Fig. 2) and the second S90, and eventually comes to the acquisition in a single shot. This magnetization is eliminated via subtraction. For the fraction which undergoes 180° rotation by the D180 (i.e., $I_{\pm} \rightarrow I_{\mp}$), the dephasing effects of the two identical encoding gradients (G_1 and G_2) are canceled, and eventually the coherence is destroyed by the gradient G_3. As a result, Cr signals that undergo various possible pathways are all suppressed.

Rigorous evaluation of the relaxation effect during the TM period is beyond the scope of the present study. The coherences that are responsible for the target signal are present at a double- or zero-quantum mode during the gradient pulses. As a further complication, during the RF pulses which primarily determine the length of TM, DQC and ZQC are interchanged via SQC and consequently the coherences may in part exhibit SQC behavior. Thus, the T_2 process during TM is likely represented by relaxation of SQC as well as those of DQC and ZQC, as implied by the phantom GSH TM T_2 (420 ms) not much shorter than the SQC T_2 (510 ms).

Lastly, the initial longitudinal magnetization of the 4.56 ppm resonance is partially affected by the water suppression RF pulses. For the present filtering scheme, since the coherence transfer between the weakly coupled 2.95 and 4.56 ppm resonances during TE_1 is negligible and the multi-quantum generation pulse (i.e., 2nd 90°) is 4.56 ppm selective, only the initial magnetization of the 2.95 ppm resonances is responsible for the filtered signal at 2.95 ppm and thus the GSH signal intensity is not influenced by the water suppression pulses. This is also the case in the study of Zhao et al. [16], and was experimentally verified in their study in comparison with the sequence of Trabesinger et al. [14,15].

In conclusion, we have demonstrated the in vivo feasibility of dual-DQC encoded filtering for measurement of GSH in the human brain. Interchange of the DQC and ZQC by a spectrally selective 180° RF pulse and subsequent encoding of the DQC enable yield enhancement of the GSH target resonance at 2.95 ppm, depending on the RF pulses and relaxation times, compared to single-DQC encoding. A proper phase cycling of the spectrally selective pulses must be incorporated to preserve the GSH target signal and cancel the overlapping resonances.

Acknowledgments

This research was supported by funds received from the State of Texas in support of the Metroplex Comprehensive Medical Imaging Center. We thank Sonya Rios for assistance with subject recruitment.

References

[1] L. Struzynska, M. Chalimoniuk, G. Sulkowski, The role of astroglia in Pb-exposed adult rat brain with respect to glutamate toxicity, Toxicology 212 (2005) 185–194.
[2] K.Q. Do, A.H. Trabesinger, M. Kirsten-Kruger, C.J. Lauer, U. Dydak, D. Hell, F. Holsboer, P. Boesiger, M. Cuenod, Schizophrenia: glutathione deficit in cerebrospinal fluid and prefrontal cortex in vivo, Eur. J. Neurosci. 12 (2000) 3721–3728.
[3] K.S. Opstad, S.W. Provencher, B.A. Bell, J.R. Griffiths, F.A. Howe, Detection of elevated glutathione in meningiomas by quantitative in vivo 1H MRS, Magn. Reson. Med. 49 (2003) 632–637.
[4] V. Govindaraju, K. Young, A.A. Maudsley, Proton NMR chemical shifts and coupling constants for brain metabolites, NMR Biomed. 13 (2000) 129–153.

[5] K. Zhong, T. Ernst, Localized in vivo human 1H MRS at very short echo times, Magn. Reson. Med. 52 (2004) 898–901.
[6] L. Hofmann, J. Slotboom, C. Boesch, R. Kreis, Characterization of the macromolecule baseline in localized ^{1}H MR spectra of human brain, Magn. Reson. Med. 46 (2001) 855–863.
[7] F. Schubert, J. Gallinat, F. Seifert, H. Rinneberg, Glutamate concentrations in human brain using single voxel proton magnetic resonance spectroscopy at 3 T, Neuroimage 21 (2004) 1762–1771.
[8] B.J. Soher, P.M. Pattany, G.B. Matson, A.A. Maudsley, Observation of coupled ^{1}H metabolite resonances at long TE, Magn. Reson. Med. 53 (2005) 1283–1287.
[9] C. Choi, P.P. Bhardwaj, P. Seres, S. Kalra, P.G. Tibbo, N.J. Coupland, Measurement of glycine in human brain by triple refocusing ^{1}H MRS in vivo at 3.0 T, Magn. Reson. Med. 59 (2008) 59–64.
[10] R.R. Ernst, G. Bodenhausen, A. Wokaun, Principles of Nuclear Magnetic Resonance in One and Two Dimensions, Clarendon Press, Oxford, 1987.
[11] P.S. Allen, R.B. Thompson, A.H. Wilman, Metabolite-specific NMR spectroscopy in vivo, NMR Biomed. 10 (1997) 435–444.
[12] M. Terpstra, P.G. Henry, R. Gruetter, Measurement of reduced glutathione (GSH) in human brain using LCModel analysis of difference-edited spectra, Magn. Reson. Med. 50 (2003) 19–23.
[13] M. Terpstra, M. Marjanska, P.G. Henry, I. Tkac, R. Gruetter, Detection of an antioxidant profile in the human brain in vivo via double editing with MEGA-PRESS, Magn. Reson. Med. 56 (2006) 1192–1199.
[14] A.H. Trabesinger, O.M. Weber, C.O. Duc, P. Boesiger, Detection of glutathione in the human brain in vivo by means of double quantum coherence filtering, Magn. Reson. Med. 42 (1999) 283–289.
[15] A.H. Trabesinger, P. Boesiger, Improved selectivity of double quantum coherence filtering for the detection of glutathione in the human brain in vivo, Magn. Reson. Med. 45 (2001) 708–710.
[16] T. Zhao, K. Heberlein, C. Jonas, D.P. Jones, X. Hu, New double quantum coherence filter for localized detection of glutathione in vivo, Magn. Reson. Med. 55 (2006) 676–680.
[17] L. Muller, Sensitivity enhanced detection of weak nuclei using heteronuclear multiple quantum coherence, J. Am. Chem. Soc. 101 (1979) 4481–4484.
[18] J. Shen, D.C. Shungu, D.L. Rothman, In vivo chemical shift imaging of γ-aminobutyric acid in the human brain, Magn. Reson. Med. 41 (1999) 35–42.
[19] A.D. Bain, Coherence levels and coherence pathways in NMR—a simple way to design phase cycling procedures, J. Magn. Reson. 56 (1984) 418–427.
[20] C. Choi, N.J. Coupland, P.P. Bhardwaj, N. Malykhin, D. Gheorghiu, P.S. Allen, Measurement of brain glutamate and glutamine by spectrally selective refocusing at 3 T, Magn. Reson. Med. 55 (2006) 997–1006.
[21] I.Y. Choi, S.P. Lee, H. Merkle, J. Shen, Single-shot two-echo technique for simultaneous measurement of GABA and creatine in the human brain in vivo, Magn. Reson. Med. 51 (2004) 1115–1121.
[22] H. Geen, X.L. Wu, P. Xu, J. Friedrich, R. Freeman, Selective excitation at two arbitrary frequencies. The double-DANTE sequence, J. Magn. Reson. 81 (1989) 646–652.
[23] G.B. Matson, An integrated program for amplitude-modulated rf pulse generation and re-mapping with shaped gradients, Magn. Reson. Imaging 12 (1994) 1205–1225.
[24] R. Gruetter, Automatic, localized in vivo adjustment of all first- and second-order shim coils, Magn. Reson. Med. 29 (1993) 804–811.
[25] R.J. Ogg, P.B. Kingsley, J.S. Taylor, WET, a T1- and B1-insensitive water-suppression method for in vivo localized ^{1}H NMR spectroscopy, J. Magn. Reson. B 104 (1994) 1–10.
[26] C. Choi, N.J. Coupland, P.P. Bhardwaj, S. Kalra, C.A. Casault, K. Reid, P.S. Allen, T_2 measurement and quantification of glutamate in human brain in vivo, Magn. Reson. Med. 56 (2006) 971–977.
[27] I.-Y. Choi, Unequivocal detection of glutathione in the human brain in vivo using navigated chemical shift imaging of glutathione: assessment of regional heterogeneity of glutathione, in: Proceedings of the 12th Annual Meeting of ISMRM, Kyoto, Japan, 2004. p. 683.
[28] V. Mlynarik, S. Gruber, E. Moser, Proton T_1 and T_2 relaxation times of human brain metabolites at 3 T, NMR Biomed. 14 (2001) 325–331.
[29] D.A. Yablonskiy, J.J. Neil, M.E. Raichle, J.J. Ackerman, Homonuclear *J* coupling effects in volume localized NMR spectroscopy: pitfalls and solutions, Magn. Reson. Med. 39 (1998) 169–178.
[30] R.A. Edden, M.G. Pomper, P.B. Barker, In vivo differentiation of *N*-acetyl aspartyl glutamate from *N*-acetyl aspartate at 3 T, Magn. Reson. Med. 57 (2007) 977–982.